Grasping Force Optimization Approaches for Anthropomorphic Hands

Aimee Cloutier
Mem. ASME
Human-Centric Design Research Lab,
Department of Mechanical Engineering,
Texas Tech University,
Lubbock, TX 79401
e-mail: aimee.cloutier@ttu.edu

James Yang[1]
Mem. ASME
Human-Centric Design Research Lab,
Department of Mechanical Engineering,
Texas Tech University,
Lubbock, TX 79401
e-mail: james.yang@ttu.edu

An appropriate choice of contact forces for anthropomorphic robotic grasping devices is important for achieving a balanced grasp. Too little applied force may cause an object to slip or be dropped, and too much applied force may cause damage to delicate objects. Prior methods of grasping force optimization (GFO) in the literature can be difficult to compare due to variability in the parameters, such as the type of grasping device, the object grasped, and the contact model, among other factors. Additionally, methods are typically tested on a very small number of scenarios and may not be as robust in other settings. This paper presents a detailed analysis of three optimization approaches based on the literature, comparing them on the basis of accuracy and computational efficiency. Numerical examples are provided for three types of grasp commonly performed by the human hand (cylindrical grasp, tip grasp, and tripod grasp) using both soft finger (SF) contact and hard finger (HF) contact friction models. For each method and grasping example, an external force is applied to the object in eighteen different directions to provide a more complete picture of the methods' performance. Contact points between the hand and the object are predetermined (given). A comparison of the results showed that the nonlinear and linear matrix inequality (LMI) approaches perform best in terms of accuracy, while the computational efficiency of the linear method is stronger unless the number of contact points and segments becomes too large. In this case, the nonlinear method performs more quickly. Future work will extend the problem of GFO to real-time implementation, and a related work (briefly addressed here) examines the sensitivity of optimization methods to variability in the contact locations. [DOI: 10.1115/1.4038684]

Keywords: Anthropomorphic hands, optimal grasping force, optimization, soft finger contact, and hard finger contact

Introduction

As robotic grasping systems become more versatile and complex, there is a growing need for robust and adaptable methods allowing these grasping devices to interact with objects. Within the scope of this problem, one important consideration is the development of automatic grasping methods resulting in adaptable and consistently stable grasps. The problem of automatic grasping has been of interest to researchers for several decades. Such considerations are applicable for a wide variety of robotic devices, including industrial robots, humanoid robots, robotic hands, and upper limb prostheses. Additionally, many robotic systems have gained the ability to interact with the environment using multiple contacts (either legs, as in a walking machine, fingers, or multiple limbs), and the principles involved in developing a grasping system are also applicable for other closed kinematic chains. Because a robotic hand's fundamental purpose is to grasp and manipulate objects, a proper choice of grasp is crucial to success in fulfilling tasks.

It is well-recognized that automatic grasping is a complex problem requiring many simplifications for reasonable implementation. Generally, automatic grasping involves the combination of several challenging tasks, including the synthesis of the optimal grasping contact points, load sharing, grasp control, grasp stability, force closure, obstacle avoidance, and task planning, among others.

While all components of the grasp planning and execution process are necessary for effective grasp, this work focuses exclusively on the optimization of grasping forces applied by the hand on the object. Effective force computation is a necessary and important consideration for the manipulation of an object by a multifingered robotic hand; further, it is critical to be able to identify appropriate grasping forces in real time. While the human hand is equipped with a complex and advanced kinematic and sensory structure which allows for natural control of contact forces and manipulation when grasping objects, the problem of choosing appropriate grasping forces for anthropomorphic robotic hands is less straightforward. Grasping force optimization (GFO) is complicated by a variety of factors, including the nonlinearity of constraints and objective functions, the relatively large number of variables and constraints, and the need to compute an optimal solution in real time. Further, some methods are acceptable for real-time computation for a small number of contact points but become unacceptable when the problem becomes more complex. Additionally, the uncertainty associated with contact locations, coefficients of friction, and the perception of object shapes due to occlusion or sensor calibration, among other factors, add complexity to the problem.

The purpose of this research is to perform a more detailed analysis of several possible grasping force optimization approaches as an extension of the work presented in Ref. [1]. The benefits and drawbacks unique to each method are compared to determine which approaches are most appropriate for determining contact forces. Namely, this work includes details regarding the tradeoff between accuracy and computational efficiency and associated factors (such as the number of segments used to approximate the friction constraint) to inform choices about which optimization approach is best. An anthropomorphic, five-fingered model of the hand is used to test the optimization approaches on a series of numerical examples representing grasps commonly performed by

[1]Corresponding author.

Manuscript received May 4, 2017; final manuscript received November 15, 2017; published online December 20, 2017. Assoc. Editor: Veronica J. Santos.

the human hand. The optimization approaches used include linear and nonlinear methods as well as the formulation of the friction constraints using linear matrix inequalities (LMIs).

One of the primary barriers to progress in GFO research has been the nonlinearity of the friction constraint represented by Coulomb's law. The most common early approach to GFO was to linearize the problem and solve for the optimal grasping forces using linear programming (LP) methods. While LP methods can be advantageous in terms of computational efficiency, they may provide grasping forces which are either too conservative or which violate the nonlinear friction constraint. Accuracy of LP methods also depends partially on how many segments are used in the linear approximation of the friction constraint. Adding more segments improves the accuracy of the solution but sacrifices computational efficiency; the computational time can become significantly larger for even a moderate number of segments. The most common LP approaches to solving the GFO problem are the simplex method [2–4] and interior point methods [5,6]. Interior point methods typically obtain solutions more quickly than the simplex method for large problems; however, they also require an initial feasible starting point.

Progress in GFO has typically been driven by breakthroughs in problem formulation, where the GFO for multifingered hands was first explored in greater depth by Kerr and Roth [7]. Buss et al. [8] discovered that the friction force constraints and force balance constraints may be represented by the positive definiteness of a certain matrix subject to linear constraints. This approach has been used by many researchers since its development and is beneficial because it retains the nonlinearity of the friction constraints without increasing the computation time unreasonably. Next, Han et al. [9] cast the friction cone constraints as LMIs and formulated the GFO problem as a convex optimization problem. The method presented by Buss et al. [8] also develops appropriate LMIs for both hard finger (HF) and soft finger (SF) friction constraints, in contrast to previous approaches. The combination of LMIs [10] and convex optimization has since been implemented by other researchers [11].

Another popular approach is to split algorithms into online and offline phases [12,13]. The computation time required during online implementation is greatly reduced by solving as much of the problem as possible offline. It is also possible to find a suboptimal but still acceptable solution to reduce computation time. Nonlinear approaches have also been studied because of their increased accuracy over LP methods. A central focus of research on nonlinear approaches is to make them fast enough for online applications. Among the most suitable approaches for real-time control and implementation are neural networks (NN). One approach of this type was developed by Xia et al. [14], where the method is able to converge to an optimal solution with any initial point. Other approaches have been developed for generic problems similar to GFO [15,16], but very few neural networks have been developed to solve the GFO problem specifically.

There are also multiple methods of decomposing contact forces for the improvement of GFO [17,18]. One such method separates the contact force into two components: the manipulation force, which contributes directly to balancing external forces applied to the object, and the internal force, which does not contribute to balancing object forces but which may be adjusted to meet other constraints [19]. Approaches have also been developed to assess the quality of a given grasp. A review of grasp quality measures is provided by Suarez et al. [20].

Currently available GFO approaches can be difficult to compare due to variable factors in the optimization approaches and in the numerical examples (e.g., object type, number of contact points, number of fingers, and contact model). In the previous work [1], the authors presented a basic examination of three methods of grasping force optimization: a linear method, a nonlinear method, and a linear matrix inequality method. As an extension of the work in Ref. [1], this paper presents a more thorough examination of three methods of GFO for anthropomorphic hands and for some grasps which have been identified as common in everyday life. Each method is tested for three different grasping scenarios, where the external force is applied to the object in eighteen different directions. The information provided presents a more complete picture about how each GFO method performs in a variety of settings.

This paper is organized as follows: First, the generic problem formulation for GFO is described. Next, the development of each specific optimization method from Ref. [1] is given. The three numerical examples are shown, along with the directions of applied forces for each example, and the sensitivity of methods with respect to variability in contact locations is briefly addressed. Results and discussion are provided for each force optimization method. Finally, concluding remarks are provided, and future work is discussed.

Grasping Force Optimization Problem Formulation

The goal of grasping force optimization is to find a set of contact forces between the hand and the object which (1) balances the object weight and other external forces applied to the object; (2) minimizes the force applied to the object by the hand contacts; and (3) meets friction, torque limit, and joint limit constraints. For the following series of equations, parameter dimensions are provided in Table 1 for a hand with n_c contacts between the hand and the object. In this paper, both HF and SF contact models are used. Table 1 provides dimensions of parameters for both contact models. Figure 1 depicts a visual representation the grasping problem, showing two arbitrary fingers j and m, where $\{N\}$ represents an inertial frame, $\{B\}$ represents the coordinate frame at the center of mass of the object, and the contact frames between the hand and the object for $i = 1, \ldots, n_c$ are represented by $\{C_i\}$. In $\{C_i\}$, n_i is an axis normal to the object, and t_i and o_i are the two axes tangential to the object. For finger i with joints 1 through k_i, $\mathbf{q}_i = [\, q_{i,1} \quad \cdots \quad q_{i,k_i} \,]^{\mathrm{T}}$ is the vector of joint angles, and $\boldsymbol{\tau}_i = [\, \tau_{i,1} \quad \cdots \quad \tau_{i,k_i} \,]^{\mathrm{T}}$ is the vector of joint torques and where $k_1 + \ldots + k_{nc} = k$ total joints for the hand, and the total vectors for joint angles and joint torques are $\mathbf{q} = [\, \mathbf{q}_1^{\mathrm{T}} \quad \cdots \quad \mathbf{q}_{n_c}^{\mathrm{T}} \,]^{\mathrm{T}}$ and $\boldsymbol{\tau} = [\, \boldsymbol{\tau}_1^{\mathrm{T}} \quad \cdots \quad \boldsymbol{\tau}_{n_c}^{\mathrm{T}} \,]^{\mathrm{T}}$, respectively (note that in Fig. 1, there are k_j joints associated with finger j and k_m joints associated with finger m). In general, a subscript i,n denotes a quantity associated with the normal axis in $\{C_i\}$. Similarly, subscripts i,t and i,o denote quantities associated with the tangential axes in $\{C_i\}$, and a subscript i,m denotes a quantity associated with the moment about the normal axis in $\{C_i\}$.

The force balance equation is shown in Eq. (1). The grasp matrix, G_i, provides a mapping between the contact wrench (i.e., a vector containing the force and moment) applied to the object by the hand in $\{C_i\}$, $\boldsymbol{\lambda}_i$, and the external wrench applied to the object, $\mathbf{g}$. The grasp matrices for individual contacts may be combined by $G^{\mathrm{T}} = [\, G_1^{\mathrm{T}} \quad \cdots \quad G_{n_c}^{\mathrm{T}} \,]$, and the individual contact wrenches are combined by $\boldsymbol{\lambda} = [\, \boldsymbol{\lambda}_1^{\mathrm{T}} \quad \cdots \quad \boldsymbol{\lambda}_{n_c}^{\mathrm{T}} \,]^{\mathrm{T}}$. A detailed derivation of G_i may be found in Ref. [20]. Equation (2) represents that acceptable joint torques may fall anywhere within the torque

Table 1 Parameter dimensions

Parameter	Dimension (HF)	Dimension (SF)
$\boldsymbol{\lambda}_i$	$\boldsymbol{\lambda}_i = [\, \lambda_{i,n} \quad \lambda_{i,t} \quad \lambda_{i,o} \,]^{\mathrm{T}}$	$\boldsymbol{\lambda}_i = [\, \lambda_{i,n} \quad \lambda_{i,t} \quad \lambda_{i,o} \quad \lambda_{i,m} \,]^{\mathrm{T}}$
$\mathbf{g}$	6×1	6×1
G	$6 \times 3n_c$	$6 \times 4n_c$
$J(\mathbf{q})$	$3n_c \times k$	$4n_c \times k$
$\boldsymbol{\tau}_e$	$k \times 1$	$k \times 1$
$\boldsymbol{\tau}$	$k \times 1$	$k \times 1$
$\boldsymbol{\tau}_L, \boldsymbol{\tau}_U$	$k \times 1$	$k \times 1$
$\mathbf{q}_L, \mathbf{q}_U$	$k \times 1$	$k \times 1$
μ_i	Scalar; for $i = 1, \ldots, n_c$	Scalar; for $i = 1, \ldots, n_c$
$\mu_{i,t}$	Scalar; for $i = 1, \ldots, n_c$	Scalar; for $i = 1, \ldots, n_c$

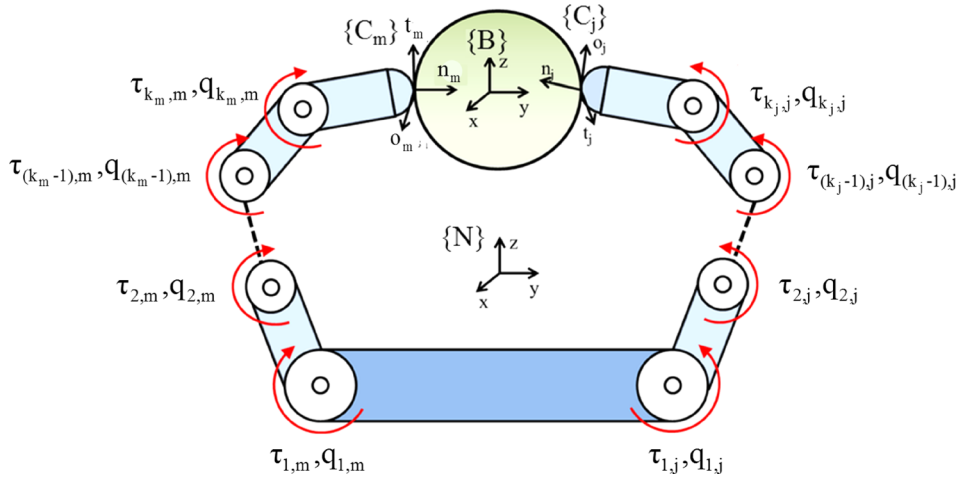

Fig. 1 Visual representation of grasping problem

limits ($\boldsymbol{\tau}_L, \boldsymbol{\tau}_U$) and Eq. (3) represents the torque balance equations; therefore, the two constraints may be combined as shown in Eq. (4). $J_i^{\mathrm{T}}(q)$ $(i = 1, \ldots, n_c)$ represents the transpose of the hand Jacobian matrix, which provides a mapping between $\{C_i\}$ and the joint coordinate frames. The hand Jacobian matrices for individual contacts may be combined by $J(\mathbf{q}) = [J_1(\mathbf{q}) \quad \cdots \quad J_{n_c}(\mathbf{q})]^{\mathrm{T}}$. Joint angles are constrained to fall within their joint limits ($\mathbf{q}_L, \mathbf{q}_U$), which is represented by Eq. (5)

$$\mathbf{g} = -G\boldsymbol{\lambda} \tag{1}$$

$$\boldsymbol{\tau}_L \leq \boldsymbol{\tau} \leq \boldsymbol{\tau}_U \tag{2}$$

$$J^{\mathrm{T}}(\mathbf{q})\boldsymbol{\lambda} = \boldsymbol{\tau} \tag{3}$$

$$\boldsymbol{\tau}_L \leq J^{\mathrm{T}}(\mathbf{q})\boldsymbol{\lambda} \leq \boldsymbol{\tau}_U \tag{4}$$

$$\mathbf{q}_L \leq \mathbf{q} \leq \mathbf{q}_U \tag{5}$$

Friction constraints may be represented in a number of different ways. Here, two contact models, HF contact and SF contact, are discussed. In the HF model, contact is represented by a point contact with friction which is capable of exerting both normal and tangential forces on the object. The HF model is represented by Coulomb's Law and is shown in Eq. (6). The SF model is useful when significant contact friction exists but allows for slight deformation between the contacts. In addition to exerting normal and tangential forces on the object, the SF contact model, shown in Eq. (7), may also generate a moment about the contact normal. HF and SF contacts are both used in this paper and impact the dimensions of $\boldsymbol{\lambda}_i$, G, and $J(\mathbf{q})$ as shown in Table 1. Finally, the normal component of the force applied to the object by each contact, $\lambda_{i,n}$, is constrained to be positive as shown in Eq. (8)

$$\sqrt{\lambda_{i,t}^2 + \lambda_{i,o}^2} \leq \mu_i \lambda_{i,n} \tag{6}$$

$$\sqrt{\frac{1}{\mu_i}\left(\lambda_{i,t}^2 + \lambda_{i,o}^2\right) + \frac{1}{\mu_{i,t}}\lambda_{i,m}^2} \leq \lambda_{i,n} \tag{7}$$

$$\lambda_{i,n} \geq 0 \tag{8}$$

The generic optimization formulation is, therefore, written as shown in Eq. (9), where f is the objective function to be minimized, and $\Im$ is used to denote the generalized friction constraint. For this problem, contact points between the hand and the object are predetermined, and appropriate joint angles are found using inverse kinematics as described in Ref. [21]. Because joint angles are known, it is unnecessary to include the joint limit constraints at this stage. The specific formulation of the problem needs adaptations depending on the quantity to be minimized and the type of optimization used. Adaptations of the problem formulation are described in the following section:

$$\begin{aligned}
&\text{find: } \boldsymbol{\lambda} = [\boldsymbol{\lambda}_1^{\mathrm{T}}, \ldots, \boldsymbol{\lambda}_n^{\mathrm{T}}]^{\mathrm{T}} \\
&\text{minimize: } f \\
&\text{subject to:} \\
&\qquad \mathbf{g} = -G\boldsymbol{\lambda} \\
&\qquad \boldsymbol{\tau}_L \leq J^{\mathrm{T}}(\mathbf{q})\boldsymbol{\lambda} \leq \boldsymbol{\tau}_U \\
&\qquad \boldsymbol{\lambda} \in \Im \\
&\qquad \lambda_{i,n} \geq 0
\end{aligned} \tag{9}$$

Optimization Approaches

Manipulation and Internal Forces. As mentioned earlier, the force applied to the object can be split into two forces, the manipulation force and the internal force, as shown in Eq. (10). In this paper, the quantity of interest to be minimized is the internal force applied to the object by contacts. From the force balance equation shown in Eq. (1), it is possible to solve for the contact wrench, $\boldsymbol{\lambda}$, as shown in Eq. (11), where G^+ is the pseudoinverse of G and $N(G)$ is the null space basis of G. The manipulation wrench, $\boldsymbol{\lambda}_{\mathrm{man}} = -G^+\mathbf{g}$, is the wrench which contributes directly to balancing $\mathbf{g}$. The wrenches which lie in the null space of G are the internal forces, $\boldsymbol{\lambda}_{\mathrm{int}}$, and can be adapted to satisfy the remaining constraints shown in Eq. (9). Manipulation forces can be solved for directly; thus, the problem can be simplified by solving for the manipulation force and using $\boldsymbol{\gamma}$ as the design variable vector and internal force as the quantity to be minimized. The dimension of $\boldsymbol{\gamma}$ is dependent on the size of the null space basis

$$\boldsymbol{\lambda} = \boldsymbol{\lambda}_{\mathrm{man}} + \boldsymbol{\lambda}_{\mathrm{int}} \tag{10}$$

$$\boldsymbol{\lambda} = -G^+\mathbf{g} + N(G)\boldsymbol{\gamma} \tag{11}$$

Problem Formulation With Nonlinear Constraints. The problem formulation which allows for nonlinear friction constraints is shown in Eq. (12), where the objective function f represents the square summation of the internal forces. Because the force balance is already satisfied by direct calculation of $\boldsymbol{\lambda}_{\mathrm{man}}$, the force balance constraint can be eliminated. The general representation of the friction constraint is $\boldsymbol{\lambda} \in \Im$; that is, the contact wrench must lie within the friction boundaries. For the HF

contact, friction constraints are represented directly by Eq. (6). For the SF contact, the friction constraints are represented by Eq. (7). The optimization problem is solved using the *fmincon* function in MATLAB

$$\begin{aligned}&\text{find: } \boldsymbol{\gamma}\\&\text{minimize: } f = \boldsymbol{\lambda}_{\text{int}}^{\text{T}}\boldsymbol{\lambda}_{\text{int}}\\&\text{subject to:}\\&\qquad \boldsymbol{\tau}_L \le J^{\text{T}}(\mathbf{q})\boldsymbol{\lambda} \le \boldsymbol{\tau}_U\\&\qquad \boldsymbol{\lambda} \in \Im\\&\qquad \lambda_{i,n} \ge 0\end{aligned} \tag{12}$$

Problem Formulation With LMIs. The second problem formulation expresses friction constraints as LMIs as presented in Ref. [4]. Detailed proofs of equivalence to the nonlinear constraints are contained in that paper; the general problem formulation using LMIs is described here.

For the friction constraints chosen for this problem, given in Eqs. (6) and (7), the formulations as LMIs are shown for HF and SF contact models in Eqs. (13) and (14), respectively, where $i = 1, \ldots, n_c$ contacts. Then, P_i for HF contact may be represented by LMIs as shown in Eq. (15), and P_i for SF contact may be represented by LMIs as in Eq. (16). Each matrix P_i may then be combined into one block diagonal matrix, P, where P_i matrices are contained along the diagonal as shown in Eq. (17). Equation (18) shows the resulting friction constraint, where 0 is a matrix of all 0 entries with the same dimensions as $P(\boldsymbol{\lambda})$

$$P_i = \begin{bmatrix} \mu_i\lambda_{i,n} & 0 & \lambda_{i,t} \\ 0 & \mu_i\lambda_{i,n} & \lambda_{i,o} \\ \lambda_{i,t} & \lambda_{i,o} & \mu_i\lambda_{i,n} \end{bmatrix} \text{ for the HF model} \tag{13}$$

$$P_i = \begin{bmatrix} \lambda_{i,n} & 0 & 0 & \frac{1}{\mu_i}\lambda_{i,t} \\ 0 & \lambda_{i,n} & 0 & \frac{1}{\mu_i}\lambda_{i,o} \\ 0 & 0 & \lambda_{i,n} & \frac{1}{\mu_{t,i}}\lambda_{i,m} \\ \frac{1}{\mu_i}\lambda_{i,t} & \frac{1}{\mu_i}\lambda_{i,o} & \frac{1}{\mu_{t,i}}\lambda_{i,m} & \lambda_{i,n} \end{bmatrix} \text{ for the SF model} \tag{14}$$

$$P_i = \lambda_{i,n}\begin{bmatrix} \mu_i & 0 & 0 \\ 0 & \mu_i & 0 \\ 0 & 0 & \mu_i \end{bmatrix} + \lambda_{i,o}\begin{bmatrix} 0 & 0 & 0 \\ 0 & 0 & 1 \\ 0 & 1 & 0 \end{bmatrix} + \lambda_{i,t}\begin{bmatrix} 0 & 0 & 1 \\ 0 & 0 & 0 \\ 1 & 0 & 0 \end{bmatrix} \tag{15}$$

$$P_i = \lambda_{i,n}\begin{bmatrix} 1 & 0 & 0 & 0 \\ 0 & 1 & 0 & 0 \\ 0 & 0 & 1 & 0 \\ 0 & 0 & 0 & 1 \end{bmatrix} + \lambda_{i,o}\begin{bmatrix} 0 & 0 & 0 & 0 \\ 0 & 0 & 0 & \frac{1}{\mu_i} \\ 0 & 0 & 0 & 0 \\ 0 & \frac{1}{\mu_i} & 0 & 0 \end{bmatrix} + \lambda_{i,t}\begin{bmatrix} 0 & 0 & 0 & \frac{1}{\mu_i} \\ 0 & 0 & 0 & 0 \\ 0 & 0 & 0 & 0 \\ \frac{1}{\mu_i} & 0 & 0 & 0 \end{bmatrix} + \lambda_{i,m}\begin{bmatrix} 0 & 0 & 0 & 0 \\ 0 & 0 & 0 & 0 \\ 0 & 0 & 0 & \frac{1}{\mu_{t,i}} \\ 0 & 0 & \frac{1}{\mu_{t,i}} & 0 \end{bmatrix} \tag{16}$$

$$P(\boldsymbol{\lambda}) = \begin{bmatrix} P_1 & 0 & 0 \\ 0 & \ddots & 0 \\ 0 & 0 & P_{n_c} \end{bmatrix} \tag{17}$$

$$P(\boldsymbol{\lambda}) \ge 0 \tag{18}$$

The new problem formulation using LMIs is shown in Eq. (19). Again, the objective function minimizes the square summation of the internal forces. Formulating the constraints both nonlinearly and as LMIs while using the same objective function will allow for a direct comparison of the computational efficiency gained through LMI constraints. Again, the problem is solved using the *fmincon* function in MATLAB

$$\begin{aligned}&\text{find: } \boldsymbol{\gamma}\\&\text{minimize: } f = \boldsymbol{\lambda}_{\text{int}}^{\text{T}}\boldsymbol{\lambda}_{\text{int}}\\&\text{subject to:}\\&\qquad \boldsymbol{\tau}_L \le J^{\text{T}}(\mathbf{q})\boldsymbol{\lambda} \le \boldsymbol{\tau}_U\\&\qquad P(\boldsymbol{\lambda}) \ge 0\\&\qquad \lambda_{i,n} \ge 0\end{aligned} \tag{19}$$

Linear Programming Method. The simplex method of linear programming has previously been used as a common method for grasping force optimization [2]. In general, the simplex method works by generating a set of all basic feasible solutions, one of which is guaranteed to be an optimum, and systematically searching these solutions to find the optimum. Computational efficiency of the simplex method is sacrificed when the number of basic feasible solutions to be inspected becomes very large. By contrast, interior point methods, some of which have been implemented in grasping force optimization, are computationally efficient but require an initial feasible solution to start the algorithm. In the previous work, several LP algorithms were tested to determine which method performed the most quickly [1]. Based on this comparison, the LP problem in this paper is solved using the *linprog* function in MATLAB with the interior point legacy algorithm.

First, it is necessary to linearize the friction constraints shown in Eq. (6). As represented in Eq. (6), the friction constraint takes the form of a quadratic cone. To linearize the constraint, Eq. (6) is approximated as a polyhedral cone. The transformation of the friction constraint is visually represented in Fig. 2, and Eq. (20) shows the force balance constraint approximated by the polyhedral cone, where T_i can be calculated for the HF contact as shown in Eq. (21) for each contact $i = 1, \ldots, n_c$ where each column for $l = 1, \ldots, n_s$ represents one segment of the polyhedral cone. n_s is the total number of segments used to create the polyhedral cone, and T_i has dimensions $3 \times n_s$ (for example, in Fig. 2, T_i approximates the cone using six segments and has dimensions 3×6). The total force balance constraint can be represented by Eq. (22), where $T = [T_1, \ldots, T_{n_c}]$, $\boldsymbol{\sigma} = [\boldsymbol{\sigma}_1^{\text{T}} \ldots \boldsymbol{\sigma}_n^{\text{T}}]^{\text{T}}$, and $\boldsymbol{\sigma} \ge 0$ (note that $\boldsymbol{\sigma}$ has dimensions of $n_s \times 1$). For this problem, it is more convenient to formulate linearized friction constraints using their dual form, represented by F, as shown in Eq. (23) and as detailed in Ref. [20]. The linearized problem formulation can be expressed as in Eq. (24)

$$G_i\boldsymbol{\lambda}_i = T_i\boldsymbol{\sigma}_i \tag{20}$$

$$T_i = \begin{bmatrix} 1 & \cdots & 1 & \cdots & 1 \\ \mu_i\cos\left(\frac{2\pi}{n_s}\right) & \cdots & \mu_i\cos\left(\frac{2l\pi}{n_s}\right) & \cdots & \mu_i\cos\left(\frac{2n_s\pi}{n_s}\right) \\ \mu_i\sin\left(\frac{2\pi}{n_s}\right) & \cdots & \mu_i\sin\left(\frac{2l\pi}{n_s}\right) & \cdots & \mu_i\sin\left(\frac{2n_s\pi}{n_s}\right) \end{bmatrix}_{3xn_s} \tag{21}$$

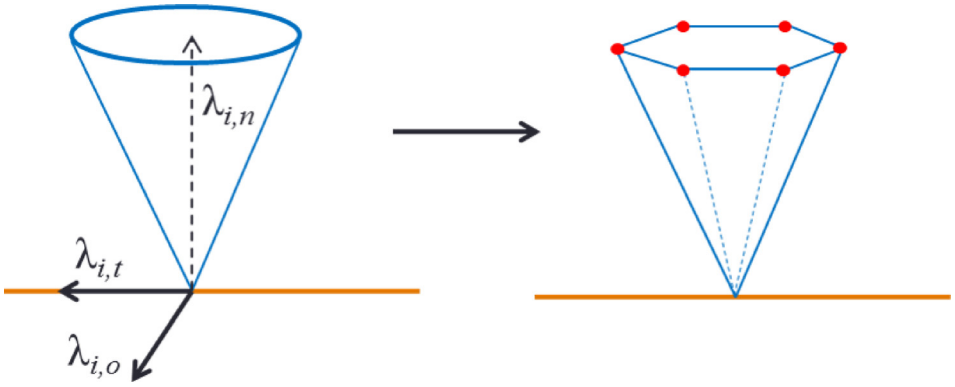

Fig. 2 Approximation of a quadratic cone as a polyhedral cone

$$G\boldsymbol{\lambda} = T\boldsymbol{\sigma} \tag{22}$$

$$F\boldsymbol{\lambda} \geq 0 \tag{23}$$

find: $\boldsymbol{\gamma}$
minimize: $f = \mathbf{c}^{\mathrm{T}}\boldsymbol{\gamma}$
subject to:

$$\begin{aligned} &\boldsymbol{\tau}_L \leq J^{\mathrm{T}}(\mathbf{q})\boldsymbol{\lambda} \leq \boldsymbol{\tau}_U \\ &F\boldsymbol{\lambda} \geq 0 \\ &\lambda_{i,n} \geq 0 \end{aligned} \tag{24}$$

Numerical Examples

Kinematics for the hand simulation were developed using the Denavit–Hartenberg method [22]. The dimensions of the palm were chosen to match the average male human hand [23], and the links of phalanges, along with upper and lower limits for each joint angle, were determined based on Ref. [24]. In total, the length of the hand is 18.9 cm and its length is 8.4 cm. Figure 3 shows a general view of the hand with a palm fixed coordinate system attached to the center of the palm which is used to define the direction of force applied to the object.

Three types of grasp which have been identified as important and frequently used in daily life are chosen for numerical examples, tip grasp, tripod grasp, and cylinder grasp [25], as shown in Fig. 4. Tip grasp and tripod grasps make contact only at the fingertips with $n_c = 2$ and $n_c = 3$, respectively, whereas cylinder grasp allows each phalanx and the palm to make contact with the object at one point ($n_c = 15$).

Varying parameters were assigned to each grasping example to test each optimization method under different conditions. All coefficients of friction were estimated based on ranges measured between the fingertips and various materials in Ref. [26]. For the tip grasp, the object is a cube with side lengths of 2.1 cm. The object mass is set to 0.1 kg with a small coefficient of friction of $\mu_i = 0.6$ for all contacts. Force is applied to the center of mass of the cube in one of 18 different directions, shown in Fig. 5 and detailed in Table 2 (in Table 2, a + indicates a force applied in the positive direction, and a– indicates a force applied in the negative direction). For the tripod grasp, the object is a cylinder with radius 2.1 cm and length 2.8 cm. The object mass is set to 1 kg with a coefficient of friction of $\mu_i = 2$ for all contacts. For the cylinder grasp, the object is a cylinder with radius 3.6 cm and length 12.6 cm. The object mass is set to 10 kg with a coefficient of friction of $\mu_i = 1$ for all contacts. The initial guesses for all cases are $\boldsymbol{\gamma} = 0$. Because the linear problem formulation is convex, its solution will provide a global optimal, whereas the nonlinear and LMI problems will yield local optimal solutions.

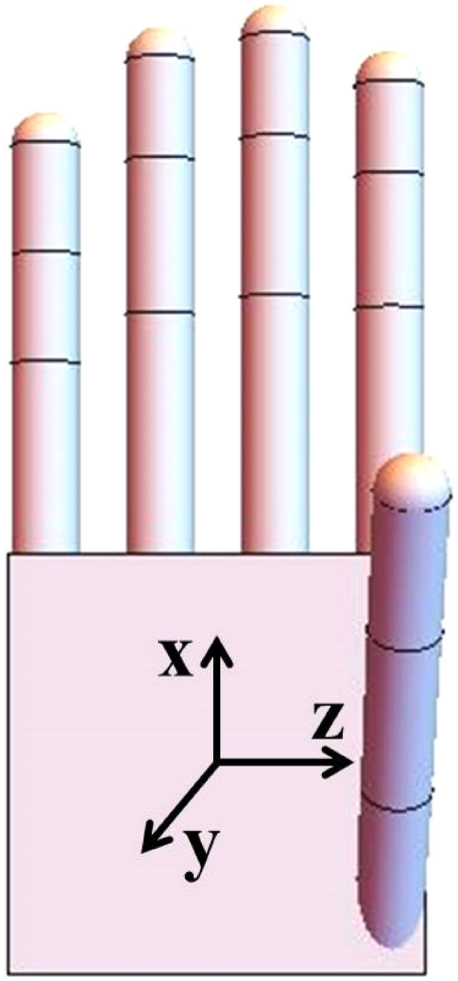

Fig. 3 Generic view of the hand

Sensitivity Analysis

In this section, a brief overview is provided of a probabilistic sensitivity analysis which was conducted to determine whether the proposed optimization methods remain robust when uncertainty in the positions of the contact locations is considered; the details of the analysis, along with complete results, are given in Ref. [27].

A Monte Carlo simulation is conducted to determine the probability of failure, i.e., the probability that a grasp cannot be maintained when variability in the contact locations is introduced. The

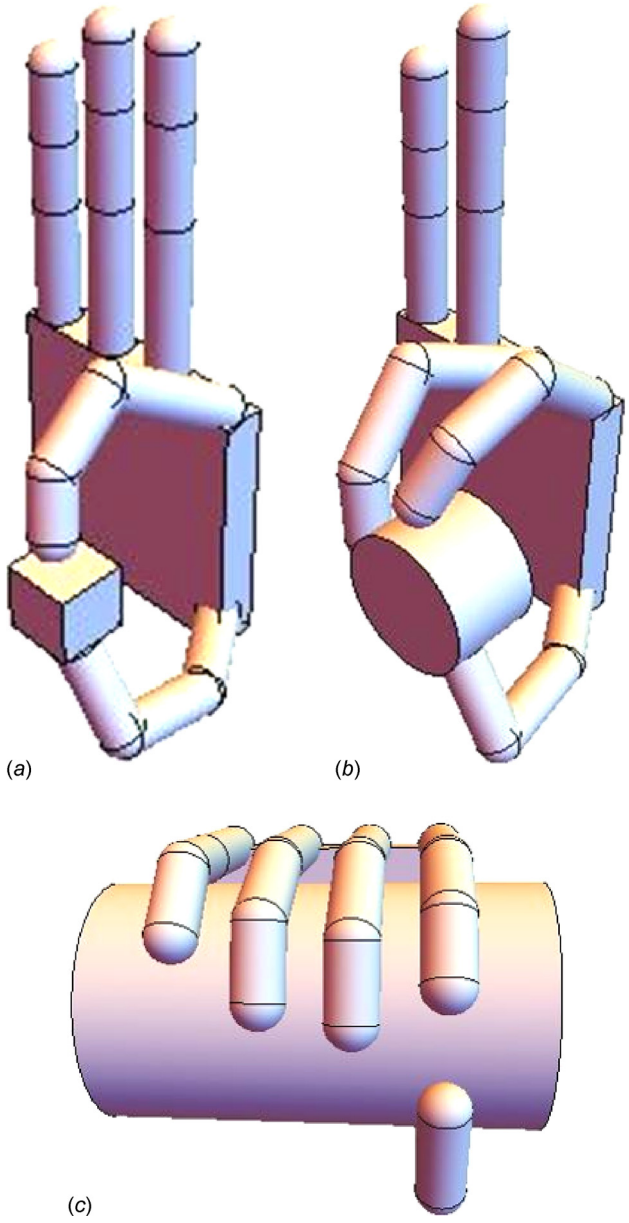

Fig. 4 Types of grasp: (*a*) tip grasp, (*b*) tripod grasp, and (*c*) cylinder grasp

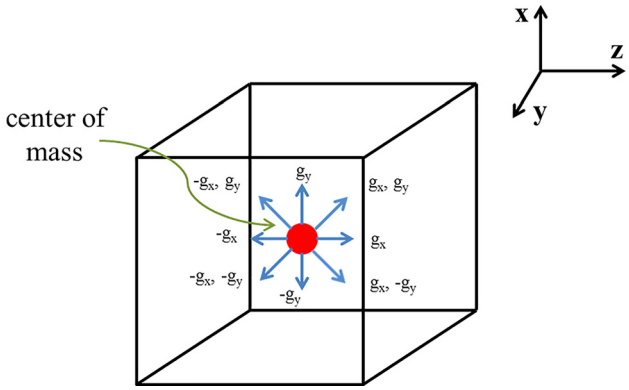

Fig. 5 Forces applied to objects

Table 2 Directions of applied forces in eighteen grasping scenarios

Force combination	g_X	g_Y	g_Z
1	+		
2	−		
3		+	
4		−	
5			+
6			−
7	+	+	
8	+	−	
9	−	+	
10	−	−	
11	+		+
12	+		−
13	−		+
14	−		−
15		+	+
16		+	−
17		−	+
18		−	−

threshold between a successful and failing result is determined based on the limit state equation, as shown in Eq. (25), where $\mathbf{f}_{\min}$ represents the minimum acceptable force required to maintain grasp and $\mathbf{f}_{\text{opt}}$ is the optimal force obtained for the deterministic solution (the solution for which no variability is considered in the contact locations). Each iteration of the Monte Carlo simulation randomly selects contact locations within the probability distributions assigned in Ref. [28], and the iteration is assessed as successful or failure. The probability of failure is then calculated as in Eq. (26), where n_{failure} is the total number of failing results and n_{samples} is the total number of iterations. Sensitivity levels are also calculated as shown in Eqs. (27) and (28) according to the method proposed in Ref. [28] to determine whether or not the probability of failure is more likely to change due to variability in a specific factor

$$\mathbf{z} = \mathbf{f}_{\min} - \mathbf{f}_{\text{opt}} \tag{25}$$

$$p_f = \frac{n_{\text{failure}}}{n_{\text{samples}}} \tag{26}$$

$$\alpha_{\mu_i} = \frac{\partial p_f}{\partial \mu_i}\left(\frac{\sigma_i}{p_f}\right) \tag{27}$$

$$\alpha_{\sigma_i} = \frac{\partial p_f}{\partial \sigma_i}\left(\frac{\sigma_i}{p_f}\right) \tag{28}$$

Results

Grasping Force Optimization. For each numerical example, the following comparisons were made: (1) difference in computation time between the HF contact and the SF contact, (2) difference in computation time among the three optimization methods (HF contact), (3) difference in computation time for the linear method with number of segments $n_s = 4, 10, 20$, (4) difference in calculated optimal forces between the HF and the SF contact, (5) difference in calculated optimal forces among the three optimization methods (HF contact), and (6) difference in calculated optimal forces for the linear method with $n_s = 4, 10, 20$.

For each direction in which force was applied, 100 examples were run with varying amounts of force in the given direction. Average values and standard deviations for computation time for all optimization methods are reported in Table 3.

Table 3 Average and standard deviation values of computation time for all grasps, in seconds

	Tip		Tripod		Cylinder	
	Average	SD	Average	SD	Average	SD
Nonlinear hard	0.026	0.040	0.030	0.045	1.66	1.18
Nonlinear soft	0.029	0.020	0.055	0.022	3.08	1.94
LMI hard	0.029	0.040	0.060	0.044	4.63	2.20
LMI soft	0.036	0.020	0.122	0.169	10.7	3.30
Linear 4 segments	0.0091	0.021	0.012	0.025	0.235	0.055
Linear 10 segments	0.011	0.024	0.017	0.036	0.716	0.226
Linear 20 segments	0.016	0.024	0.052	0.090	3.52	1.31

Several patterns emerge from the data shown in Table 3. First, the nonlinear method consistently solves the problem more quickly than the LMI method. For tip grasp, when there are only two contact points with the object, the difference is small but becomes much larger as the number of contact points increases. The linear method also solves the problem more quickly than the nonlinear and LMI methods in most cases. Exceptions occur for the tripod and cylinder grasps, where the nonlinear method solves more quickly than the linear method using $n_s = 20$. In all cases, the computation time grows as more contact points are considered, and it grows substantially when whole hand grasp is considered; many of the computation times shown for the cylinder grasp are too slow for practical application. Similarly, in the case of whole hand grasp, the computation time grows quickly as the number of segments used to linearize the friction constraint becomes larger. The difference is so significant that the nonlinear method actually outperforms the linear method when the number of segments becomes too large. Finally, methods which use the HF contact model consistently solve more quickly than the SF model. So, if the optimal forces calculated for the HF and SF contact are similar, it would make sense to use the HF contact model since the computation time is smaller.

Tables 4–7 show some sample results of the forces computed for the tip grasp and cylinder grasp, considering both the HF and the SF contact. Results are presented in Newtons in terms of $\boldsymbol{\lambda}$, the grasping force in the contact frames. In general, for the HF contact, $\boldsymbol{\lambda}$ takes the form $\boldsymbol{\lambda} = [\lambda_{1,n}\ \lambda_{1,t}\ \lambda_{1,o} \cdots \lambda_{n_c,n}\ \lambda_{n_c,t}\ \lambda_{n_c,o}]^{\mathrm{T}}$. For the tip grasp, the object is contacted in two places ($n_c = 2$). Similarly, results for the SF contact are shown for two methods (the approximation of SF contact for the linear case is not presented here) where $\boldsymbol{\lambda}$ takes the form $\boldsymbol{\lambda} = [\lambda_{1,n}\ \lambda_{1,t}\ \lambda_{1,o}\ \lambda_{1,m} \cdots \lambda_{n_c,n}\ \lambda_{n_c,t}\ \lambda_{n_c,o}\ \lambda_{n_c,m}]^{\mathrm{T}}$. In Table 6, only the rows with the significantly large differences between the nonlinear and linear cases are included; all other results are eliminated for brevity, as there are 15 contacts between the hand and the object for cylinder grasp. Similarly, in Table 7, only the rows with the largest differences between the nonlinear and LMI cases are shown. In Tables 6 and 7, the rows with the largest differences between the HF contact and the SF contact for the nonlinear case are shown in bold.

For all optimization methods presented in Tables 4 and 5, the forces meet the expected constraints (normal force must be nonnegative, normal and tangential forces must fall within friction constraint boundaries). For tip grasp, the nonlinear and LMI results are identical in both the HF and SF contact cases. The normal forces for the linear methods differ from those for nonlinear and LMI methods but become acceptably close as the number of segments increases from 4 to 20. It is also notable that in the SF case, the additional term which represents the moment about the normal does not contribute much to the applied forces.

Table 5 Representative data for tip grasp, SF contact

		Nonlinear	LMI
Thumb	$\lambda_{1,n}$(N)	0.841	0.841
	$\lambda_{1,t}$(N)	−0.234	−0.234
	$\lambda_{1,o}$(N)	0.047	0.047
	$\lambda_{1,m}$(N)	0.00099	0.00099
Index	$\lambda_{2,n}$(N)	0.841	0.841
	$\lambda_{2,t}$(N)	−0.251	−0.251
	$\lambda_{2,o}$(N)	−0.438	−0.438
	$\lambda_{2,m}$(N)	−0.0001	−0.0001

For the HF contact, the nonlinear and LMI results remain very close, while for SF contact, certain results differ much more significantly. In general, there is good agreement between the nonlinear and LMI methods about which phalanges of the fingers need to apply force (in most cases, the phalanges for which the forces are very close to zero are the same), but there are differences in the magnitudes of the forces, which typically differ by 2 or 3 N. For the HF contact, once again, there is a good agreement between nonlinear and linear methods about which phalanges need to apply forces, but the differences in magnitudes are in the 4–5 N range. Most notably, the force applied by the middle finger, distal phalanx is substantially different between the nonlinear and linear cases. For most contact points, the results for the three linear cases do not change much as the number of segments changes. For this reason, differences between the linear and nonlinear cases may be attributed to differences in the objective function rather than insufficient segments to approximate the friction constraint.

Tables 8 and 9 show the percent differences among optimization methods for tip and tripod grasps and HF contact, where representative percent differences are shown considering all force directions. Table 8 shows very small differences in the optimal forces calculated using the nonlinear and LMI methods for HF contact, and the differences between the nonlinear and linear methods become smaller as the number of segments increases. When using 20 segments to approximate the friction constraint, all differences are below 1%.

For tripod grasp, the results produced by the nonlinear and LMI methods are very small. In general, the percent difference between nonlinear and linear methods also decreases as more segments are used to approximate the friction cone. The differences are larger for tripod grasp than for tip grasp but are still always below 15%. However, it is also notable that for the middle finger contact point, the percent difference actually increases as more segments are used.

Probabilistic and Sensitivity Analysis. A brief summary of the major results of the probabilistic and sensitivity analysis is

Table 4 Representative data for tip grasp, HF contact

		Nonlinear	LMI	Linear, 4 segments	Linear, 10 segments	Linear, 20 segments
Thumb	$\lambda_{1,n}$(N)	0.827	0.827	1.29	0.879	0.842
	$\lambda_{1,t}$(N)	−0.245	−0.245	−0.247	−0.246	−0.246
	$\lambda_{1,o}$(N)	0.051	0.051	−0.050	0.039	0.047
Index	$\lambda_{2,n}$(N)	0.827	0.827	1.29	0.879	0.842
	$\lambda_{2,t}$(N)	−0.240	−0.240	−0.238	−0.240	−0.240
	$\lambda_{2,o}$(N)	−0.435	−0.435	−0.536	−0.446	−0.438

Table 6 Representative data for cylinder grasp, HF contact

		Nonlinear	LMI	Linear, 4 segments	Linear, 10 segments	Linear, 20 segments
Thumb, proximal phalanx	$\lambda_{1,n}$(N)	6.70	6.70	5.01	3.94	4.01
	$\lambda_{1,t}$(N)	2.44	2.45	4.54	3.80	3.94
	$\lambda_{1,o}$(N)	2.98	2.99	−0.475	−0.448	−0.460
Index, distal phalanx	$\lambda_{5,n}$**(N)**	**6.53**	**6.53**	**6.92**	**6.76**	**6.79**
	$\lambda_{5,t}$**(N)**	**−6.52**	**−6.52**	**−6.87**	**−6.75**	**−6.79**
	$\lambda_{5,o}$**(N)**	**−0.270**	**−0.271**	**−0.050**	**0.028**	**0.020**
Middle, middle phalanx	$\lambda_{7,n}$(N)	0.00086	0.00052	5.16	4.91	4.93
	$\lambda_{7,t}$(N)	−0.00039	−0.00044	−5.11	−4.90	−4.92
	$\lambda_{7,o}$(N)	0.000016	−0.000025	−0.050	0.0280	0.019
Middle, distal phalanx	$\lambda_{8,n}$(N)	14.8	14.8	6.79	6.57	6.55
	$\lambda_{8,t}$(N)	−14.8	−14.8	−6.67	−6.56	−6.55
	$\lambda_{8,o}$(N)	−0.461	−0.466	−0.118	0.027	0.0045
Ring, distal phalanx	$\lambda_{11,n}$(N)	17.8	17.8	21.8	23.7	23.7
	$\lambda_{11,t}$(N)	−17.8	−17.8	−21.7	−23.7	−23.7
	$\lambda_{11,o}$(N)	−0.511	−0.510	−0.082	0.031	0.018
Pinky, distal phalanx	$\lambda_{13,n}$**(N)**	**6.78**	**6.78**	**5.58**	**5.10**	**5.07**
	$\lambda_{13,t}$**(N)**	**−6.77**	**−6.78**	**−5.53**	**−5.09**	**−5.07**
	$\lambda_{13,o}$**(N)**	**−0.194**	**−0.195**	**−0.050**	**0.028**	**0.020**
Palm contacts	$\lambda_{15,n}$(N)	22.4	22.4	27.1	26.9	27.0
	$\lambda_{15,t}$(N)	22.4	22.4	27.0	27.0	27.0
	$\lambda_{15,o}$(N)	−0.825	−0.823	−0.050	0.028	0.0081

Table 7 Representative data for cylinder grasp, SF contact

		Nonlinear	LMI
Thumb, proximal phalanx	$\lambda_{1,n}$(N)	6.67	5.56
	$\lambda_{1,t}$(N)	4.72	1.85
	$\lambda_{1,o}$(N)	0.013	0.011
	$\lambda_{1,m}$(N)	0.377	0.665
Index, distal phalanx	$\lambda_{5,n}$**(N)**	**10.5**	**8.12**
	$\lambda_{5,t}$**(N)**	**−10.5**	**−8.12**
	$\lambda_{5,o}$**(N)**	**−0.00065**	**−0.00083**
	$\lambda_{5,m}$**(N)**	**−0.046**	**−0.057**
Middle, distal phalanx	$\lambda_{8,n}$(N)	16.1	13.4
	$\lambda_{8,t}$(N)	−16.1	−13.4
	$\lambda_{8,o}$(N)	−0.003	−0.002
	$\lambda_{8,m}$(N)	−0.054	−0.068
Ring, distal phalanx	$\lambda_{11,n}$(N)	15.2	12.7
	$\lambda_{11,t}$(N)	−15.2	−12.7
	$\lambda_{11,o}$(N)	−0.00027	−0.00188
	$\lambda_{11,m}$(N)	−0.0483	−0.05974
Pinky, distal phalanx	$\lambda_{13,n}$**(N)**	**2.30**	**0.338**
	$\lambda_{13,t}$**(N)**	**−2.29**	**−0.338**
	$\lambda_{13,o}$**(N)**	**−0.00054**	**0.00014**
	$\lambda_{13,m}$**(N)**	**−0.020**	**−0.0049**
Palm contacts	$\lambda_{15,n}$(N)	25.2	12.8
	$\lambda_{15,t}$(N)	25.2	35.9
	$\lambda_{15,o}$(N)	−0.0057	−0.0033
	$\lambda_{15,m}$(N)	0.077	0.155

presented in this section, where complete details of the results may be found in Ref. [27]. Table 10 shows the probabilities of failure for each method and grasp under investigation. The main observation which can be drawn from these results is that the nonlinear and LMI optimization methods remain significantly more robust to variability in contact locations than the linear method; even despite increasing the number of segments used to approximate the friction constraint, the linear method remains far from acceptable for use in grasping force optimization.

Discussion

In general, the nonlinear method seems to have the best compromise of computation speed and accuracy. Although the linear method performs more quickly for a small number of segments or a small number of fingers, differences occur between the nonlinear and linear methods due to an insufficient number of segments or variability in the objective functions. Also, for a large number of contacts and a large number of segments, the nonlinear method has better accuracy and better computation time compared to the linear method. For whole hand grasp, significantly large differences were also observed between the HF and the SF contact. Despite these differences, it is likely that HF contact is still a better approach due to the difference in computation time between the two methods.

A number of possible challenges exist when implementing GFO methods to control a real robotic hand. One significant factor affecting the control of an artificial hand would be the sensitivity of the presented methods to changes or errors in the contact location. The authors have conducted a detailed examination of this

Table 8 Percent differences among optimization types, tip grasp, HF contact

		Nonlinear versus LMI	Nonlinear versus linear, 4	Nonlinear versus linear, 10	Nonlinear versus linear, 20
Thumb	$\lambda_{1,n}$(N)	1.07×10^5	38.0	5.52	0.902
	$\lambda_{1,t}$(N)	6.6×10^8	0.288	0.035	0.0056
	$\lambda_{1,o}$(N)	1.07×10^5	38.0	5.53	0.903
Index	$\lambda_{2,n}$(N)	1.07×10^5	38.0	5.52	0.902
	$\lambda_{2,t}$(N)	6.7×10^8	0.293	0.035	0.0057
	$\lambda_{2,o}$(N)	1.07×10^5	38.0	5.53	0.903

Table 9 Percent differences among optimization types, tripod grasp, HF contact

		Nonlinear versus LMI	Nonlinear versus linear, 4	Nonlinear versus linear, 10	Nonlinear versus linear, 20
Thumb	$\lambda_{1,n}$(N)	2.71×10^5	9.90	2.38	3.07
	$\lambda_{1,t}$(N)	5.11×10^8	0.030	0.011	0.0051
	$\lambda_{1,o}$(N)	4.28×10^5	26.3	11.6	8.85
Index	$\lambda_{2,n}$(N)	4.41×10^5	26.6	1.87	2.41
	$\lambda_{2,t}$(N)	7.8×10^9	0.0065	0.0060	0.0097
	$\lambda_{2,o}$(N)	3.72×10^5	15.7	4.27	7.26
Middle	$\lambda_{3,n}$(N)	6.39×10^5	10.4	13.8	14.4
	$\lambda_{3,t}$(N)	4.7×10^7	0.287	0.132	0.109
	$\lambda_{3,o}$(N)	0.00018	340.6	71.3	10.6

Table 10 Probabilities of grasp failure

	LMI	Nonlinear	Linear (4 seg)	Linear (10 seg)	Linear (20 seg)
Tip grasp					
Hard	1.2%	0.5%	43.3%	39.5%	38.6%
Soft	1.2%	0.5%	—	—	—
Tripod grasp					
Hard	0.0%	0.0%	99.9%	47.85	41.7%
Soft	0.0%	0.0%	—	—	—

problem, presented in Ref. [27] and briefly discussed in this work, consisting of Monte Carlo simulations to identify both the probability of failure (where "failure" indicates that the constraints of the problem are violated, and the grasp cannot be maintained) and sensitivity levels when variability in the contact locations is considered. Two major results emerged from this analysis. First, the nonlinear and LMI methods both remain robust for all grasps when contact location variability is introduced (probabilities of failure, at a maximum, are 2% and are often significantly less), whereas the linear method, in general, is likely to yield higher probabilities of failure. Second, the probability of failure is likely to be higher, regardless of the optimization method, when the grasp becomes less restrictive, i.e., the highest probabilities of failure occur for tip grasp when the number of contact points between the hand and the object is lowest. The results presented in Ref. [27] complement and strengthen the results of this paper by showing that two of the optimization methods remain viable when variability is introduced; further, combining the results of the analysis presented in this work and the results presented in Ref. [27], the nonlinear method emerges clearly as the most appropriate approach since it requires less computation time than the LMI method. Additional details on the sensitivity of the methods presented here to changes in the contact location may be found in Ref. [27].

Other factors which may affect the control of the real robotic hand include the sensitivity of sensors to measure forces and contact points as well as the requirements for these sensors. It is crucial to identify these and other factors which may affect the implementation of GFO methods. The validation of these results using experimental methods is, therefore, a necessary subsequent step in this work.

Additionally, the numerical examples presented in this paper deal only with static forces. Realistically, an artificial hand must be capable of adapting to variable loads. Future work will include an extension of the methods presented here (focusing primarily on the nonlinear, HF contact method) to find solutions when the external force applied to the object varies. Other methods similar to this formulation will also be explored to improve computational efficiency for online implementation. The nonlinear, HF contact method will also be compared to a neural network to determine which approach is more appropriate. A suboptimal approach or an approach which splits the problem into offline and online components may be beneficial for obtaining solutions more quickly. It would also be desirable to allow the hand to change contact locations (i.e., manipulate an object) after contact has been established. Future work will also explore methods of computing optimal grasping forces combined with object manipulation.

Conclusion

In this paper, a detailed examination of the three methods to predict optimal grasping forces in Ref. [1] was presented for three common types of grasps performed by anthropomorphic artificial hands. A probabilistic and sensitivity analysis was carried out. In general, the nonlinear method using the HF contact performed with the best combination of accuracy and computation speed, although the linear method was often more efficient except when the number of segments and contacts between the hand and the object became too large. However, in conjunction with the sensitivity analysis considering variability in the contact locations conducted in Ref. [28], the nonlinear method emerges clearly as the most appropriate optimization method since the linear method, in general, does not remain robust to changes in the contact locations. Future work will include extending the methods presented in this paper to cases for which the external load applied to the object varies and comparing them to a neural network. Additionally, methods of combining object manipulation with optimal force calculation will be explored.

Funding Data

- CH Foundation (2012).
- NSF Graduate Research Fellowship (1356111).

References

[1] Cloutier, A., and Yang, J., 2016, "Force Optimization Approaches for Common Anthropomorphic Grasps," ASME Paper No. DETC2016-60346.
[2] Cheng, F. T., and Orin, D. E., 1990, "Efficient Algorithm for Optimal Force Distribution—The Compact-Dual LP Method," IEEE Trans. Rob. Autom., **6**(2), pp. 178–187.
[3] Klein, C. A., and Kittivatcharapong, S., 1990, "Optimal Force Distribution for the Legs of a Walking Machine With Friction Cone Constraints," IEEE Trans. Rob. Autom., **6**(1), pp. 73–85.
[4] Zheng, Y., Chew, C. M., and Adiwahono, A. H., 2011, "A GJK-Based Approach to Contact Force Feasibility and Distribution for Multi-Contact Robots," Rob. Auton. Syst., **59**(3–4), pp. 194–207.
[5] Boyd, S. P., and Wegbreit, B., 2007, "Fast Computation of Optimal Contact Forces," IEEE Trans. Rob., **23**(6), pp. 1117–1132.
[6] Zheng, Y., Lin, M. C., and Manocha, D., 2010, "A Fast n-Dimensional Ray-Shooting Algorithm for Grasping Force Optimization," IEEE International Conference on Robotics and Automation (ICRA), Anchorage, AK, May 3–7, pp. 1300–1305.
[7] Kerr, J., and Roth, B., 1986, "Analysis of Multifingered Hands," Int. J. Robotics Res., **4**(4), pp. 3–17.
[8] Buss, M., Hashimoto, H., and Moore, J. B., 1996, "Dexterous Hand Grasping Force Optimization," IEEE Trans. Rob. Autom., **12**(3), pp. 406–418.
[9] Han, L., Trinkle, J. C., and Li, Z. X., 2000, "Grasp Analysis as Linear Matrix Inequality Problems," IEEE Trans. Rob. Autom., **16**(6), pp. 663–674.
[10] Liu, G., and Li, Z., 2004, "Real-Time Grasping Force Optimization for Multifingered Manipulation: Theory and Experiments," IEEE/ASME Trans. Mechatronics, **9**(1), pp. 65–77.

[11] Lippiello, V., Siciliano, B., and Villani, L., 2013, "A Grasping Force Optimization Algorithm for Multiarm Robots With Multifingered Hands," IEEE Trans. Rob., **29**(1), pp. 55–67.
[12] Zheng, Y., and Qian, W. H., 2006, "A Fast Procedure for Optimizing Dynamic Force Distribution in Multifingered Grasping," IEEE Trans. Syst., Man, Cybern.—Part B: Cybern., **36**(6), pp. 1417–1422.
[13] Zuo, B. R., and Qian, W. H., 2000, "A General Dynamic Force Distribution Algorithm for Multifingered Grasping," IEEE Trans. Syst., Man, Cybern.—Part B: Cybern., **30**(1), pp. 185–192.
[14] Xia, Y., Wang, J., and Fok, L. M., 2004, "Grasping-Force Optimization for Multifingered Robotic Hands Using a Recurrent Neural Network," IEEE Trans. Rob. Autom., **20**(3), pp. 549–554.
[15] Sun, J., Chen, J. S., and Ko, C. H., 2012, "Neural Networks for Solving Second-Order Cone Constrained Variational Inequality Problem," Comput. Optim. Appl., **51**(2), pp. 623–648.
[16] Miao, X., Chen, J. S., and Ko, C. H., 2014, "A Smoothed NR Neural Network for Solving Nonlinear Convex Programs With Second-Order Cone Constraints," Inf. Sci., **268**, pp. 255–270.
[17] Bicci, A., 1993, "Force Distribution in Multiple Whole-Limb Manipulation," IEEE International Conference on Robotics and Automation (ICRA), Atlanta, GA, May 2–6, pp. 196–201.
[18] Zhang, Y., and Gruver, W. A., 1995, "Definition and Force Distribution of Power Grasps," IEEE International Conference on Robotics and Automation (ICRA), Nagoya, Japan, May 21–27, pp. 1373–1378.
[19] Xu, J., Wang, M. Y., Wang, H., and Li, Z., 2007, "Force Analysis of Whole Hand Grasp by Multifingered Robotic Hand," IEEE International Conference on Robotics and Automation (ICRA), Roma, Italy, Apr. 10–14, pp. 211–216.
[20] Suarez, R., Roa, M., and Cornella, J., 2006, "Grasp Quality Measures," Polytechnic University of Catalonia, Barcelona, Spain, accessed Dec. 13, 2017, http://citeseerx.ist.psu.edu/viewdoc/download?doi=10.1.1.278.4317&rep=rep1&type=pdf
[21] Fu, K. S., Gonzalez, R. C., and Lee, C. S. G., 1987, *Robotics: Control, Sensing, Vision, and Intelligence*, McGraw-Hill, New York.
[22] Denavit, J., and Hartenberg, R. S., 1955, "A Kinematic Notation for Lower-Pair Mechanisms Based on Matrices," ASME J. Appl. Mech., **23**, pp. 215–221.
[23] Chandra, A., Chandra, P., and Deswal, S., 2011, "Analysis of Hand Anthropometric Dimensions of Male Industrial Workers of Haryana State," Int. J. Eng., **5**(3), pp. 242–256.
[24] Pena-Pitarch, E., Yang, J., and Abdel-Malek, K., 2005, "SANTOS^{TM} Hand: A 25 Degree-of-Freedom Model," SAE Paper No. 2005-01-2727.
[25] Dalley, S. A., Wiste, T. E., Varol, H. A., and Goldfarb, M., 2010, "A Multigrasp Prosthesis for Transradial Amputees," IEEE Engineering Medical Biology Society, pp. 5062–5065.
[26] Tomlinson, S. E., Lewis, R., and Carre, M. J., 2007, "Review of the Frictional Properties of Finger-Object Contact When Gripping," J. Eng. Tribol., **221**(8), pp. 841–850.
[27] Cloutier, A., 2017, "Grasping Force Optimization Approaches for Common Anthropomorphic Grasps," Ph.D. dissertation, Texas Tech University, Lubbock, TX.
[28] Das, P. K., and Zhang, W., 2003, *Guidance on Structural Reliability Analysis of Marine Structures*, University of Glasgow, Glasgow, Scotland.